

DESIGN AND LIFE ESTIMATION OF BLISK IN GAS TURBINES

M.SAI LAKSHMI¹, Dr. V. NAGA BHUSHANA RAO²

¹M.tech Student, Department of Mechanical Engineering, Raghu Institute of Technology, Visakhapatnam

²Professor, Department of Mechanical Engineering, Raghu Institute of Technology, Visakhapatnam

Abstract- *The gas turbine is the heart of all modern marine propulsion. The present study deals with the fatigue analysis of a turbine disc (Integrated blade and disc) for a small gas turbine for a short life application. The role of the turbine blisk in a gas turbine is to expand the hot gases which come out from the combustion chamber and to provide the necessary thrust required, for the propulsion of the marine vehicle. Due to high rotational speeds the blisk is subjected to high centrifugal loads. This blisk experiences varying stress amplitudes. Therefore the turbine blisk is the most critical part in a gas turbine engine. It also develops the power required to drive the compressor and other accessories. This paper describes design modeling, structural and dynamic analysis of BLISK in gas turbines. In this paper, the Blisk of gas turbine has been modeled in CATIA V6 software. Further 8 different design models of the Blisk have been developed, so as to find the best model based on the results obtained from static structural analysis using ANSYS 18.0. Then Stress analysis has been carried out by the application of the boundary conditions and loads on the modified model using three different materials namely IN738, IN718 and NiCr8020. Three types of fillet radius are considered to avoid the corner stress between disk and blade. The results from the analyses are studied to give the best material which is suitable to determine the fatigue life and factor of safety of the modified Blisk by using relevant formulae.*

Keywords: Blisk, Gas turbine, Fatigue Analysis Stress Analysis, Static Analysis, Modal Analysis ,Dynamic Analysis.

1. Introduction

A gas turbine is a manufactured machine that exploits the mechanical work created by the continuous combustion of an air/fuel mix. Air is swallowed at the intake of the engine by the fan. In engines without bypass, all the air enters the core of the engine. Otherwise, a fraction of the air flow bypasses the core of the engine. The core flow passes through several stages of the low pressure compressor (LPC). On three-shaft engines, the fan is the only stage of the LPC and the air subsequently goes through an intermediate pressure compressor (IPC). This flow is compressed further in the high pressure compressor (HPC) before it is mixed with fuel. This mix burns in the combustion chamber and hot gases are then expanded in

the high pressure turbine (HPT), the intermediate pressure turbine (IPT), if any, and the low pressure turbine (LPT). Each compressor is driven by its own turbine stage(s) which gives a control of its angular speed. From high to low angular speeds one finds the HPC/HPT, the IPC/IPT, if any, and the LPC/LPT. The power transmitted to the driving shafts is only a small fraction of the power produced by the engine. A turbo machine is made of a static casing attached to the vessel or the ground inside which two or three shafts are rotating concentrically, with contra-rotation in some engines. In the engine the inner shaft connects the fan and the LPC to the LPT. The outer shaft connects the HPC to the HPT. In compressors and turbines, the air flows through interlaced rotor and cantilevered or mobile stator vanes. A blisk is a turbo machine component comprising both rotor disk and blades. It consists of a single part, instead of an assembly of a disk and individual, removable blades. Blisks may be integrally cast, machined from a solid piece of material, or made by welding individual blades to a rotor disk. The term is used mainly in aerospace engine design. Blisks may also be known as integrally bladed rotors. The main advantage is that instead of making bare compressor disks and attaching the blades later, blisks are single elements combining the two. This eliminates the need to attach the blades to the disk (via screws, bolts, etc.), thus decreasing the number of components in the compressor, while at the same time decreasing drag and increasing efficiency of air compression in the engine. The elimination of the dovetail attachment found on traditional turbine blades eliminates a source for crack initiation and subsequent propagation.

2. Literature review

This chapter presents a review of the technical literature to the issue that related in design and development of turbine blisk. The chapter reviews about the history of turbine blisk.

Chan and Tuba [1] analyzed the effect of the blade/disc clearance and the frictional forces on the stress distribution in the blade root fastening. It was shown that the coefficient of friction had a slight yet distinguishable effect on both the maximum fillet stresses and on the load distribution at the teeth flanks. Changes in clearance revealed more significant effects compared to those obtained by contact friction.

Zboinski [2] developed a computer program for the FE analysis of three-dimensional non-linear contact problems. The algorithm utilized the variation principle of incremental frictional contact mechanics. A simplified FE analysis of a four teeth fir-tree region of turbo machinery was performed by simple tension and bending. The results revealed that the maximum tensile stress due to tension and bending occurs at the base of the tooth closest to the disc. Thermal analysis were not taken into account

Papanikos, Meguid and Stjepanovic [3] developed a FE del to examine the effect of the critical geometric features and interface conditions on the stress field at the blade/disc interface for an aero engine compressor disc under centrifugal loading. Their results indicated that the maximum stress occurs just below the lower contact point. The results also showed that variations in the geometry and coefficient of friction effect the stress distribution at the blade/disc interface. This work concluded that three dimensional models gave more accurate stress distribution compared to two dimensional analysis Furthermore, it was shown that the skew angle can significantly influence the stress distribution at the blade disc interface.

Meguid et ai. [4] Analyzed the structural integrity of dovetail joints by initiating and tracking the propagation of cracks in aero engine disc subjected to centrifugal loading. It was observed that peak stresses occurs just below the lower contact point of the last tooth. For the disc geometry studied by Meguid, crack propagation took place across the throat region and not through the disc and the stress intensity factor at the crack tip was of the mixed mode type.

Singh and Ratwani [5] suggested an approach to analyze the fir-tree region of a turbine disc subjected to centrifuga1 loading. Their method treated the total fir-tree region as an assembly of several steps. Using a generalized root step, the analysis was conducted to obtain its stiffness and deflection using the FE method. Several of these root steps were later assembled to form a fir-tree region of a disc. The loads carried by each step were then calculated by solving a set of linear algebraic equations. This work suffers from too many approximations.

Papers [6-20], the characteristics of Blisk in gas turbines using static and modal analyses are studied.

3. Problem Identification and Objective

Blisk must possess enough strength to withstand all the forces and loads acting on it statically and dynamically. Life of an element depends on the selection of material properties. Thermal deformation and thermal stresses to

be minimized by using high resistive materials. Maximum stresses are observed at corner location of blisk.

The objective is to carry out fluid structural interface analysis of turbo machinery turbine integrated blade rotor. The law of physics cannot be directly applied onto real systems to avoid complexity. So, the assumptions are made to convert the physical model into required geometric model. Thus this geometric model is used to analyze the motion of a system by approximation of its dynamic behavior.

Dynamic analysis of blisk means study of the fatigue analysis and responses of structures with its material parameters and analyzing them for any defect. Four high temperature resistive materials are used to find out the thermal deformation and thermal stresses. Maximum stresses are observed at corner location of blisk and these can be avoided using geometric fillet are placed between disk and blades. Four types of fillet radius are considered. The results of the analyses are studied to give the best material to be used for the modified model of Turbine Blisk.

4. Design of Blisk Blade profile

The first step in designing a turbine is to select the velocity triangles at mean radius, and subsequently the radial variation of the triangles. Mo The design iterations showed that a rotor of 160 mm diameter was required for delivering a mass flow rate of 1.896 kg/s at a rotational speed of 1168 rpm. The tip speed was limited to 346 m/s based on mechanical integrity. Considering the axial inlet Mach number for the design as 0.4, the minimum blade height required for this design was estimated to be 21 mm.

as well as inlet flow angle α_1 is taken as 65.23 0 , outlet angle is 41.660

4.1 Material Properties

Three different materials were used for the analysis of the Blisk to know the best material for the chassis. The properties of the materials are shown below.

Parameter		IN 718	NiCr 8020	IN 738
young's modulus	G.Pa	200	245	149
UTS	M.Pa	1034	1020	1158
Yield strength	M.Pa	1000	950	1027
Max working stress	M.Pa	637	945	443
R.A	%	35	25	25

Table 1: Material Properties

The above image shows the finite element model of water domain and turbine blisk. Here tetra hadrons element is used to mesh the domain and blisk. Connection between blisk and domain has clearly checked to avoid the turbulent flow. After the meshing we have 78216 nodes and 8561 elements.

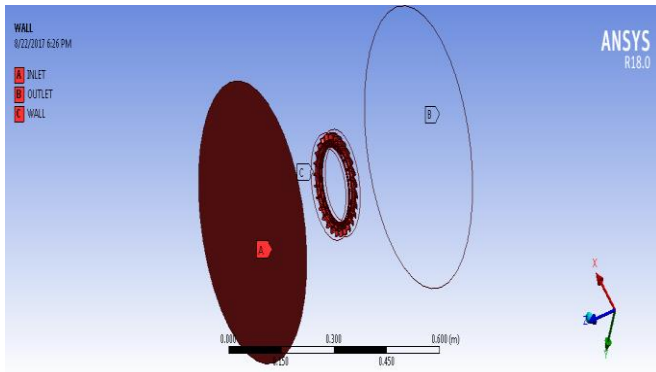


Fig 5: Inlet of fluent domain

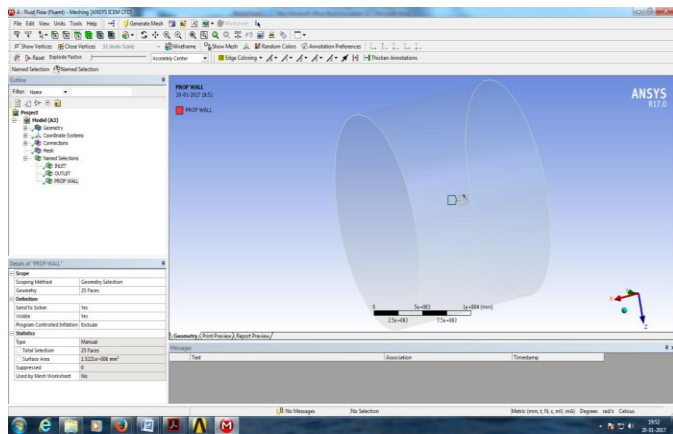


Fig 6: Symmetry Condition of Fluent Domain

Boundary conditions are used according to the need of the model. The inlet and outlet conditions are defined as velocity inlet and pressure outlet. The walls are separately specified with respective boundary conditions. No slip condition is considered for each wall. The details about all boundary conditions can be seen below.

Gas inlet temp = $877^{\circ}\text{C} = 1150\text{ K}$

Velocity in gas= 160 m/sec

Blade rotation = 1168

The number of iteration is set to 500 and the solution is calculated and various contours, vectors and plots are obtained.

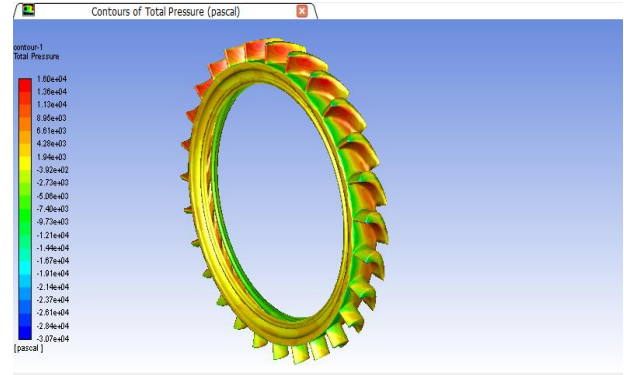


Fig 7: Pressure contour on blisk.

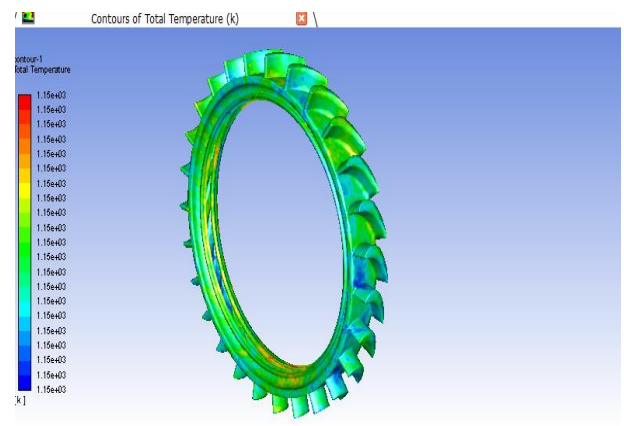


Fig 8: Temperature contour on turbine blisk.

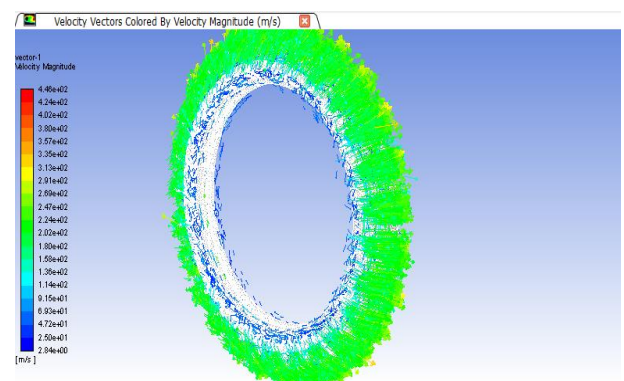


Fig 9: vector velocity distribution on blisk.

6. FINITE ELEMENT ANALYSIS:

ANSYS 18.0 is used to run the analysis. The previously created IGS file is imported on ANSYS file geometry. Solid mesh is used to divide the geometric body in to small strips (Finite elements). Fixed boundary conditions are applied.

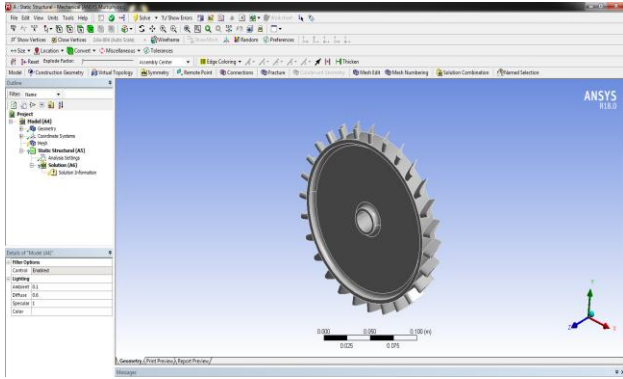


Fig 10: Geometry model of turbine blisk.

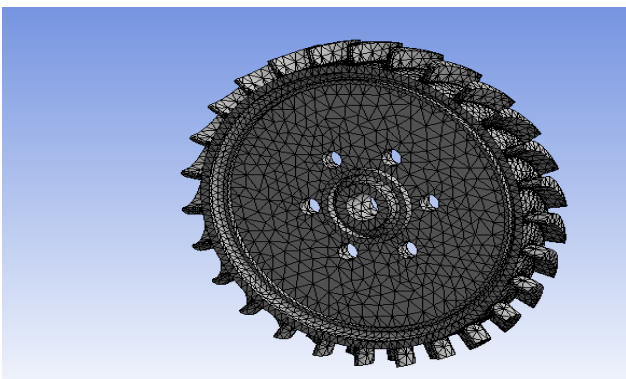


Fig 11: Finite element model of blisk.

It is an important technique in Finite element methods. Generally mesh 200 element is available in the ANSYS workbench. These elements are used to solve in the shell and solid element. When there is number of element present we can get the exact results. At the same time, hexagonal meshing gives best results.

Boundary conditions and loading:

There are different types of boundary conditions that can be applied to edge or faces.

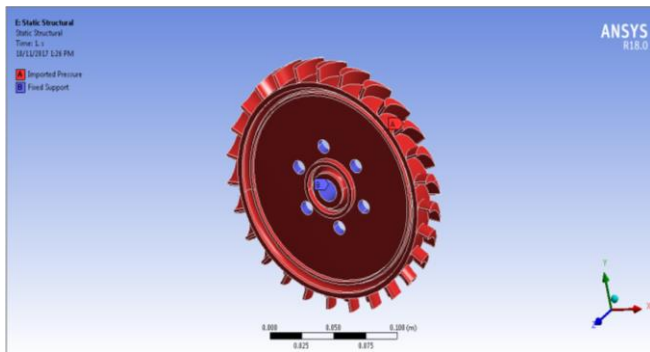


Fig 11: Boundary condition on blisk

In ANSYS, static structure and modal analysis are performed. The table which is shown below, different materials for different components are used bicycle seat assembly. Solid mesh 200 element are used to divide the geometric body in to small strips (Finite elements)

Parameter		IN 718	NiCr 8020	IN 738
young's modulus	G.Pa	200	245	149
UTS	M.Pa	1034	1020	1158
Yield strength	M.Pa	1000	950	1027
Max working stress	M.Pa	637	945	443
R.A	%	35	25	25

Table-2: Blisk material properties

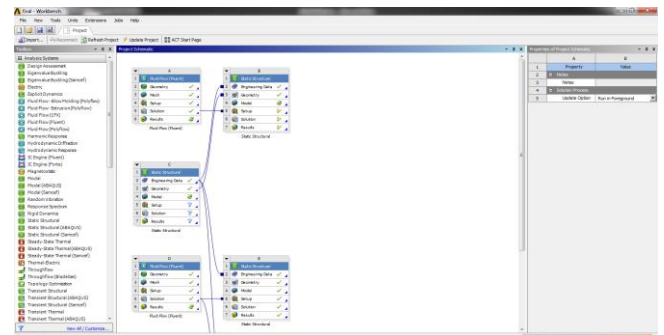


Fig 12: Planning to run the analysis.

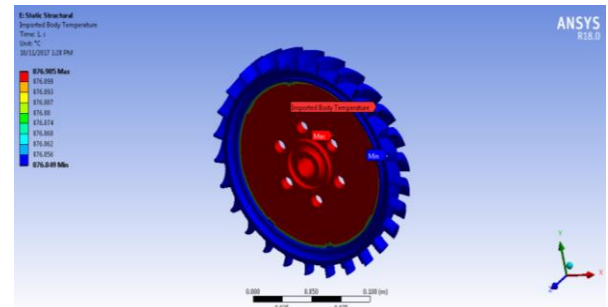


Fig 13: Thermal loading imported into structural analysis.

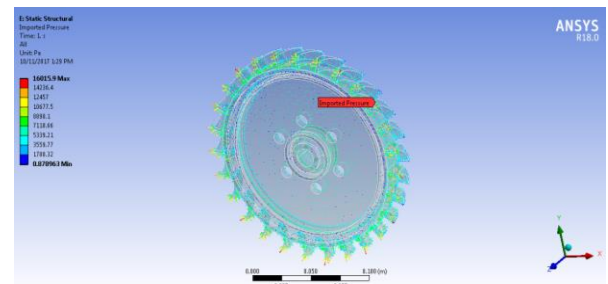


Fig 14: Pressure loading imported into structural analysis.

Deformation in the material (IN 718):

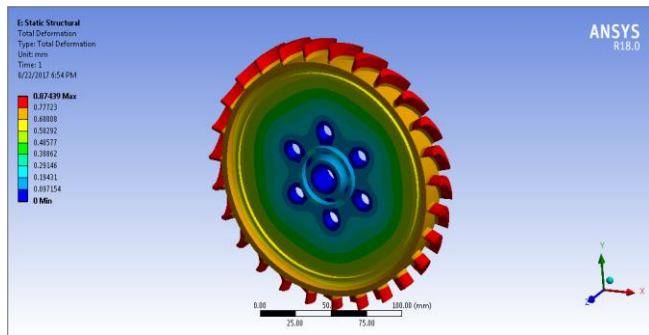


Fig 15: Deformation of Blisk (IN-718)

In the above image shows the total deformation of blisk (IN-718) after dynamic load 0.16 MPa load applied on face of blisk and the red indicate the maximum deformation and blue indicates minimum deformation. Maximum deformation occurs at the tip of blade because there is no support at tip, so there is a high chance of the blade to get bent. Minimum deformation appears at the hub of the propeller and we can clearly able to see in the above image. All together maximum deformation is 0.87 mm. This deformation is much of considerable deformation.

Stresses in the material (IN 718):

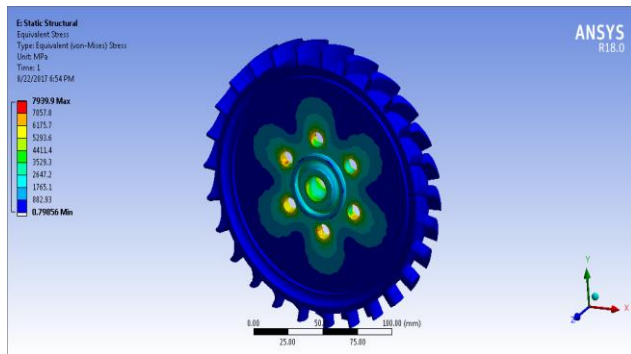


Fig 16: Stresses on blisk (IN-718)

The above figure shows stresses on blisk (IN-718) when applied dynamic pressure. In this the blue indicates for minimum stresses and red indicates for maximum stresses. All over the blisk, minimum stresses are occurred. There are more stresses occurring at the connection between disk and blade. The entire part is safely under the design limit. But maximum stresses are present mainly in the sharply corners of the disk.

Stresses on Blade (IN 718):

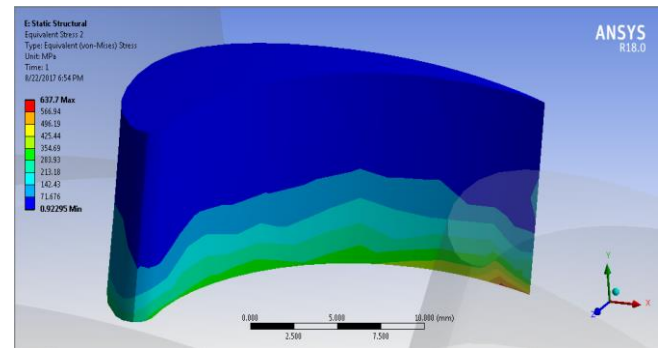


Fig 17: Stresses on blade (IN-718)

The above figure shows stresses on blade (IN-718) when applied dynamic pressure. In this the blue indicates for minimum stresses and red indicates for maximum stresses. All over the blade, minimum stresses are occurred. There are more stresses occurring at the connection between disk and blade. The entire part is safely under the design limit. But maximum stresses are present mainly in the sharply corners of the disk.

The above mentions models with three different materials IN-718, IN-738 and NiCr-8020 were analysed and result are studied.

1mm Fillet on the blade:

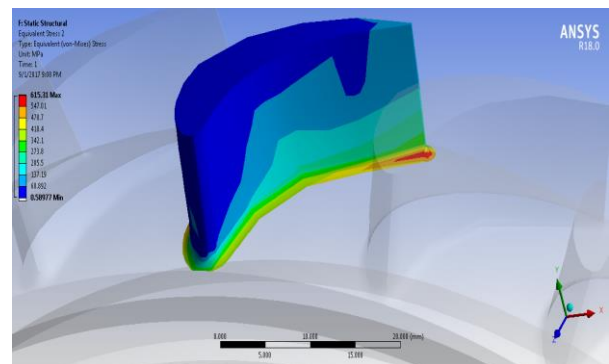


Fig18: Thermal stresses of blade (fillet 1mm, In718 material)

The above figure shows strain on blade at different materials when applied dynamic pressure. In this the blue indicates for minimum strain and red indicates for maximum strain. All over the blade, minimum Thermal stresses are occurred. There are more stresses occurring at the connection between disk and blade. The entire part is safely under the design limit. But maximum stresses are present mainly in the sharply corners of the disk. Thermal stresses by adding 1 mm fillet on the blade is 615.31mpa

The above mentions models with three different fillets with 1 mm, 0.75mm, and 0.50mm for the materials IN-718, IN-738 and NiCr-8020 were analyzed and results are studied.

7. FATIGUE ANALYSIS:

It is the progressive and localized structural damage that occurs when a material is subjected to cyclic loading. The nominal maximum stress values that cause such damage may be much less than the strength of the material typically quoted as the ultimate tensile stress limit, or the yield stress limit.

The stress analysis and fatigue life for the given materials have been carried out under maximum temperature and steady state conditions. For all the three materials under consideration the operating speed of 1168 RPM has been kept constant.

The factor of safety has been determined by the following formula,

Factor of safety = Yield Strength / Maximum Working Stress.

The fatigue life for the materials conducted has been obtained using Coffin-Manson Equation. The fatigue life and factor of safety of all the materials have been determined as follows

Coffin Manson equation is

$$E_t = \frac{3.5 \times UTS}{E} N_f^{-0.12} + D_t^{0.6} \times N_f^{-0.6}$$

$$D_t = -\ln(1 - RA)$$

Where, UTS is Ultimate Tensile Strength

RA is Reduction of Area

E is Young's Modulus

E_t is total mechanical strain

N_f is Number of fatigue cycle

D_t is ductility

Calculation for In718 Material:

$$D_t = -\ln(1 - RA)$$

$$D_t = -\ln(1 - 0.35)$$

$$=0.43.$$

$$E_t = \frac{2.5 \times 1158}{149e3} N_f^{-0.12} + 0.43 \times N_f^{-0.6}$$

$$0.011=0.0272 N_f^{-0.12} + 0.43 \times N_f^{-0.6}$$

Mechanical Strain is calculated from Ansys software i.e., 0.011 mm/mm.

Number of cycles from the equation is 12000.

Calculation for In738 Material:

$$D_t = -\ln(1 - RA)$$

$$D_t = -\ln(1 - 0.25)$$

$$=0.287.$$

$$E_t = \frac{2.5 \times 1034}{200e3} N_f^{-0.12} + 0.287 \times N_f^{-0.6}$$

$$0.01=0.0181 N_f^{-0.12} + 0.287 \times N_f^{-0.6}$$

Mechanical Strain is calculated from Ansys software i.e., 0.01 mm/mm.

Number of cycles from the equation is 2500.

Calculation For NiCr Material:

$$D_t = -\ln(1 - RA)$$

$$D_t = -\ln(1 - 0.25)$$

$$=0.287.$$

$$0.013=0.0146 N_f^{-0.12} + 0.287 \times N_f^{-0.6}$$

Mechanical Strain is calculated from Ansys software i.e., 0.013 mm/mm. Number of cycles from the equation is 1500.

Theoretical calculation for different fillet radius:

Calculation For 0.5 mm fillet:

$$D_t = -\ln(1 - RA)$$

$$D_t = -\ln(1 - 0.35)$$

$$=0.43.$$

$$E_t = \frac{2.5 \times 1158}{149e3} N_f^{-0.12} + 0.43 \times N_f^{-0.6}$$

$$0.01074 = 0.0272 N_f^{-0.12} + 0.43 \times N_f^{-0.6}$$

Mechanical Strain is calculated from Ansys software i.e., 0.01074 mm/mm.

Number of cycles from the equation is 13210.

Calculation For 0.75 mm fillet:

$$D_t = -\ln(1 - RA)$$

$$D_t = -\ln(1 - 0.35)$$

$$= 0.43.$$

$$E_t = \frac{2.5 \times 1158}{149e3} N_f^{-0.12} + 0.43 \times N_f^{-0.6}$$

$$0.010644 = 0.0272 N_f^{-0.12} + 0.43 \times N_f^{-0.6}$$

Mechanical Strain is calculated from Ansys software i.e., 0.010644 mm/mm.

Number of cycles from the equation is 13812.

Calculation For 1 mm fillet:

$$D_t = -\ln(1 - RA)$$

$$D_t = -\ln(1 - 0.35)$$

$$= 0.43.$$

$$E_t = \frac{2.5 \times 1158}{149e3} N_f^{-0.12} + 0.43 \times N_f^{-0.6}$$

$$0.01059 = 0.0272 N_f^{-0.12} + 0.43 \times N_f^{-0.6}$$

Mechanical Strain is calculated from Ansys software i.e., 0.01059 mm/mm.

Number of cycles from the equation is 14101.

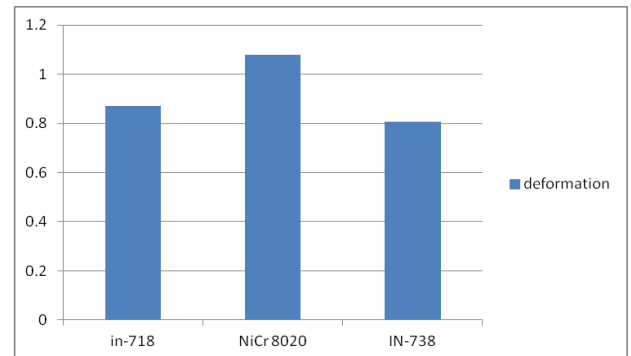
8. RESULTS AND DISCUSSION:

Total blisk model is created as single component in CATIA software and model was imported into ANSYS software. Fluent analysis is performed to find out the temperature and hydro dynamic pressure. Dynamic hydraulic pressure loading is considered such as 0.6 MPa.

In static structural analysis, the results are shown below

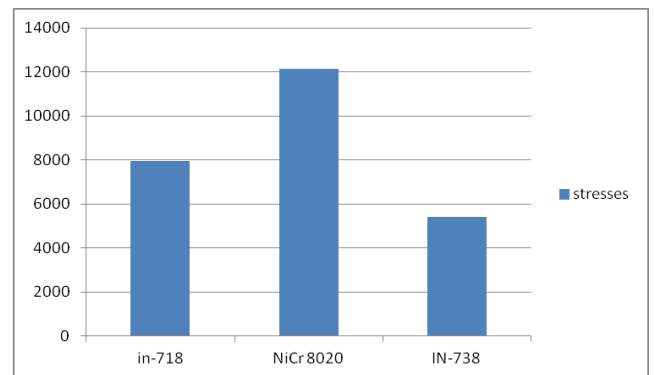
Parameter	IN-718	NiCr 8020	IN-738
Deformation	0.87	1.079	0.805
Stresses	7939	12127	5415
stress on blade	637	945	443
strain on blade	0.01087	0.006846	0.007664

Table 3: Different material results



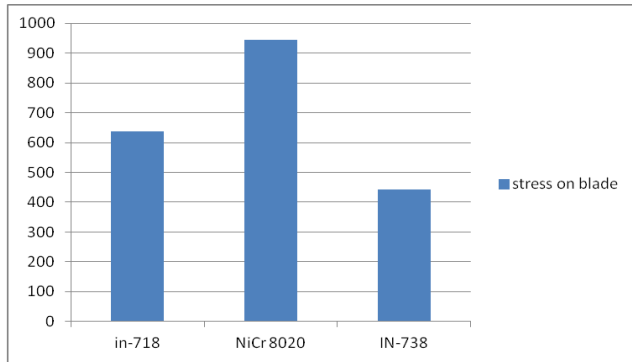
Graph 1: deformation for different materials.

The above graph shows the deformation of blisk for different material. The X-axis shows the materials such as IN-718, NiCr-8020 and IN-738. The Y-axis denotes for the deformation of blisk. In the material IN-718 shows the deformation occurs nearly at 9mm, while the for material NiCr-8020 the deformation occurs nearly at 1.01mm and for the material IN-738 the deformation occurs at 0.8mm.



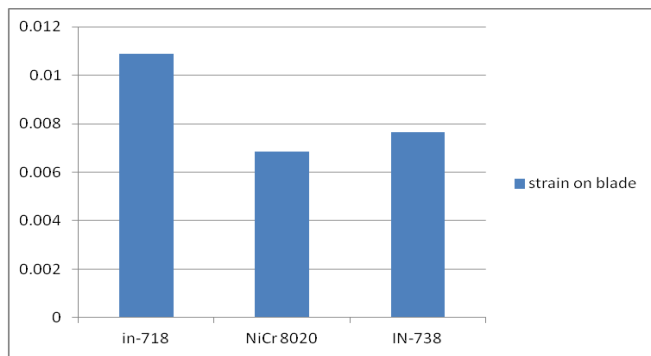
Graph 2: Stresses for different materials.

The above graph shows the stresses of blisk for different material. The X-axis shows the materials such as IN-718, NiCr-8020 and IN-738. The Y-axis denotes for the stress of blisk in MPa. In the material IN-718 shows the stress occurs nearly at 7900 MPa, while the for material NiCr-8020 the stress occurs nearly at 1200 MPa and for the material IN-738 the stresses occurs at 5500 MPa.



Graph 3: Stresses on blade for different materials.

The above graph shows the stresses of blade for different material. The X-axis shows the materials such as IN-718, NiCr-8020 and IN-738. The Y-axis denotes for the stress of blade in MPa. In the material IN-718 shows the stress occurs nearly at 620 MPa, while for the material NiCr-8020 the stress occurs nearly at 950 MPa and for the material IN-738 the stresses occurs at 420 MPa.

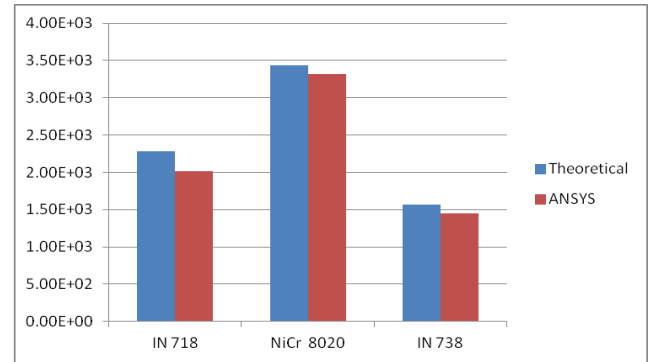


Graph 4: Strain on blade for different materials.

The above graph shows the strain of blade for different material. The X-axis shows the materials such as IN-718, NiCr-8020 and IN-738. The Y-axis denotes for the deformation of blade. In the material IN-718 shows the strain occurs nearly at 0.011 mm/mm, while for the material NiCr-8020 the strain occurs nearly at 0.00653mm/mm and for the material IN-738 the strain occurs at 0.0071 mm/mm.

Material	Theoretical	ANSYS
IN 718	2.28E+03	2020
NiCr 8020	3433.92	3315
IN 738	1566.288	1450

Table 4: comparison between theoretical and ANSYS (only temperature loading).



Graph 5: comparison between theoretical and ANSYS (only temperature loading).

The above graph shows the comparison between theoretical and ANSYS. Theoretical results are performed using thermal stresses formula i.e.

$$stress = E \times \alpha \times \Delta T$$

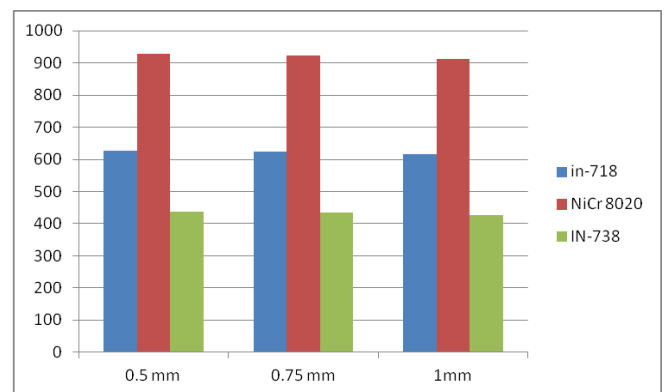
E= young's modulus of material.

α = thermal expansion

ΔT = change in temperature

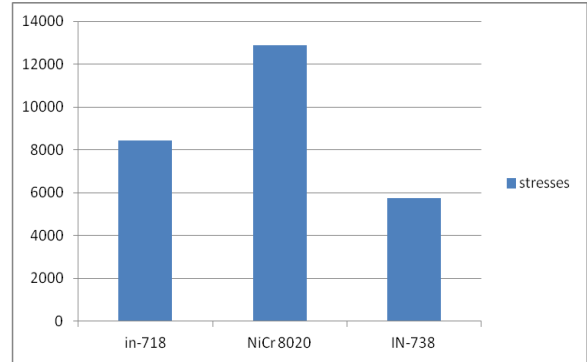
stresses on the blade			
fillet radius	0.5 mm	0.75 mm	1mm
in-718	626	623	615
NiCr 8020	929	924	912
IN-738	436	434	427

Table 5: stresses of blade with different fillet radius



Graph 6: stresses of blade with different fillet radius and materials.

The above graph shows the stresses at different material that are maintained with different fillet radius to avoid the stress concentration. In X-direction shows the different materials such as IN-718, NiCr-8020, IN-738 and Ti. In the Y-direction the fillet radius are 0.5mm, 0.75mm and 1mm are given. For the material IN-718 the maximum stress occurred in 0.5mm fillet radius which is 610 MPa, medium stress occurred in 0.75 fillet radius at 605 MPa and minimum stress occurred in 1mm fillet radius of 600 MPa. For NiCr-8030 maximum stresses occurred is higher than other material. Whereas for the the fillet radius 0.5mm the maximum stress occurred at 920 MPa, for the fillet radius 0.75mm the medium stress occurred at 910mm and for 1mm fillet radius the minimum stress occurred at 905 MPa. For IN-738, for the 0.5mm and 0.75mm fillet radius the maximum stresses occurred at 420MPa and the minimum stresses occurred at 405 MPa.

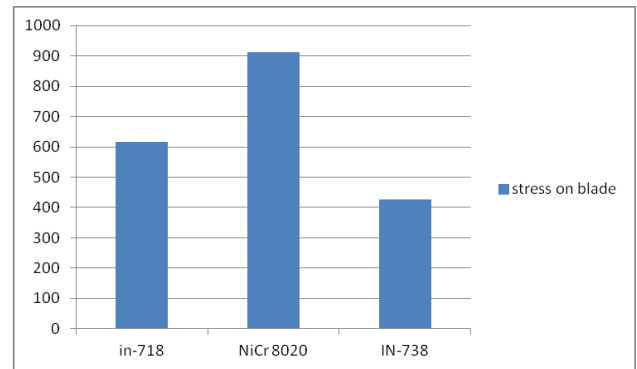


Graph 8: Stresses for fillet radius 1 mm

The above graph show the stress occurred at different material for fillet radius of 1mm. The x-direction is for the materials like IN-718, NiCr-8020, IN-738 and Ti. The Y-Direction is for the stress in MPa. For the material IN-718 the stress occurred at 8200 MPa, for NiCr-8020 the stress occurred in 128500 MPa, for IN-738 the stress occurred at 5800 MPa.

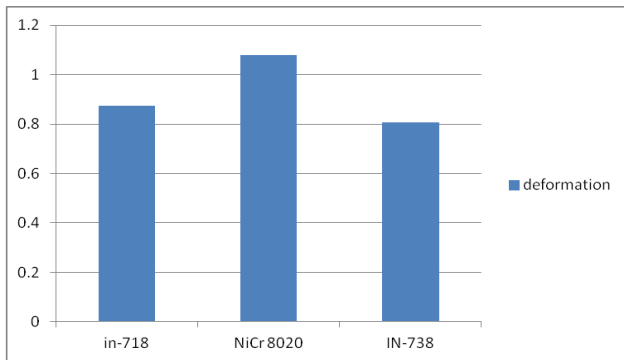
stresses on Blade for fillet radius 1 mm			
Parameter	in-718	NiCr 8020	IN-738
Deformation	0.874	1.079	0.805
Stresses	8439	12887	5757
stress on blade	615	912	427

Table 6: stresses on Blade for fillet radius 1 mm



Graph 9: stresses on Blade for fillet radius 1 mm

The above graph show the stress on blade occurred at different material for fillet radius of 1mm. The x-direction is for the materials like IN-718, NiCr-8020, IN-738 and Ti. The Y-Direction is for the stress in MPa. For the material IN-718 the stress occurred at 610 MPa, for NiCr-8020 the stress occurred in 920 MPa, for IN-738 the stress occurred at 420 MPa.

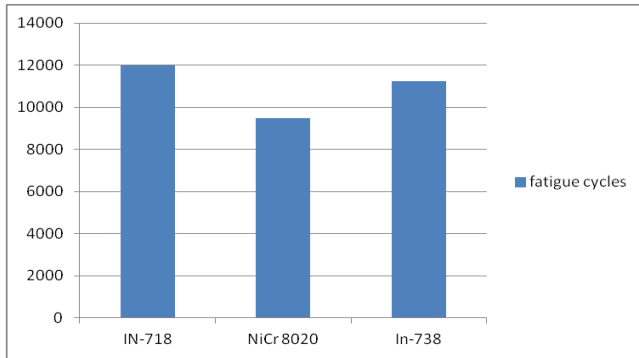


Graph 7: Deformation on Blade for fillet radius 1 mm

The above graph show the deformation occurred at different material for fillet radius of 1mm. The x-direction is for the materials like IN-718, NiCr-8020, IN-738 and Ti. The Y-Direction is for the deformation in mm. For the material IN-718 the deformation occurred at 0.85mm, for NiCr-8020 the deformation occurred in 1.01mm, for IN-738 the deformation occurred at 0.8mm.

Materials	Fatigue cycles
IN-718	12000
NiCr 8020	9500
In-738	11252

Table 7: Fatigue cycles of blisk blades

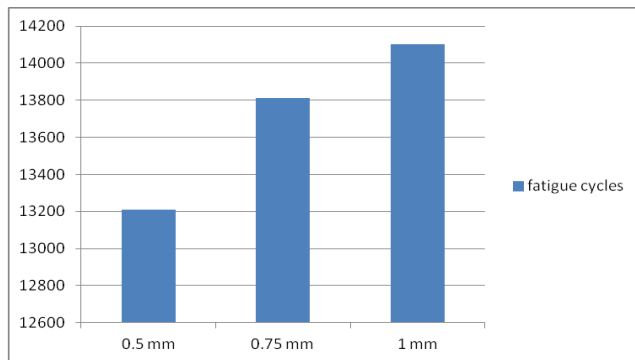


Graph 10: Fatigue cycles of blisk blades

The above Graph shows the fatigue cycles of blisk blade at different material properties. Here maximum possible cycles are having in IN-718 materials and minimum number of cycles to failure is having in Ni-Cr materials.

fillet radius	fatigue cycles
0.5 mm	13210
0.75 mm	13812
1 mm	14101

Table 8: Fatigue cycles of blisk blades with different fillet radius.



Graph 11: Fatigue cycles of blisk blades with different fillet radius.

The above Graph shows the fatigue cycles of blisk blade at different fillet radius. Here maximum possible cycles are having in 1mm fillet radius and minimum number of cycles to failure is having in 0.5mm fillet.

9. RESULTS:

The main aim of the project is to select the best material which has better fatigue life among the three materials IN 718, IN738 and NiCr8020 considered for the future production of the turbine blisk.

To achieve this, a model of turbine blisk has been created using CATIA and analysis is performed in ANSYS and later the fluid structural analysis has been carried out.

Fluid structure interface analysis is performed and maximum stress induced in IN738 as compared to remaining materials.

The maximum stress level experienced, factor of safety and fatigue life cycle of the blisk under thermal loading, are better for IN-718 compared to IN738 and NiCr8020.

The Factor of safety (FOS) and fatigue life cycle (No) of IN718 has been found to be 1.58 and 12458 cycles respectively.

10. CONCLUSION:

The following conclusions have been drawn from the analysis.

It is evident from the results of analysis that under given speed, temperature and geometry, the thermal stresses induced in the blade region are within the permissible limits for all the three materials.

The maximum von misses stress induced has been lesser than the yield strength which suggests that the design is safe for all the three materials.

Hence it is concluded that IN 718 is a better material based on Fatigue Analysis when compared to IN738 and NiCr8020 and can be used for future production and applications of turbine blisk.

11. SCOPE FOR FUTURE WORK:

For the given model the deformation, stresses and life may be analyzed by making following changes,

1. By increasing the hub thickness of disk we can reduce the stresses of blisk.
2. Selection of high thermal resistance material needed to prepare the blisk. Because maximum stresses in gas turbine blades are only due to thermal condition.
3. Blade angles, Height and thickness are main parameters to reduce the thermal stresses in blade.

12. REFERENCES:

1. Chan S. K. and Tuba L S., A Finite Element method for Contact Problems of Solid Bodies - Part II: Applications to Turbine Blade Fastenings, International Journal of Mechmical Science, v. 13, pp. 627 - 639, 1971.

2. Zboinski G., Finite element computer program for incremental analysis of large three dimension frictional contact problems of linear elasticity, *Computers and Structures*, v.46, n.4, pp 679 - 687, 1993.
3. Papanikos P., Meguid S. A. and Stjepanovic Z., Three dimensional nonlinear finite element analysis of dovetail joints in aero engine discs, *Finite Element in Analysis and Design*, Vol. 29, 1998.
4. Meguid S. A., Refaat M. H. and Papanikos P., Theoretical and experimental studies of structural integrity of dovetail joints in aero engine discs, *Journal of Materials Technology*, Vol. 56, pp. 1539 - 1547, 1996.
5. Singh G. D. and Rawtani S., Fir tree fastenings of turbomachines, *bfudes - 1: Deflection analysis*, *International Journal of Mechanical Science*, Vol. 24, no. 6, pp. 377 - 384, 1982.
6. Sarlashkar A. K., Lam T. and McCloskey T. H., B lude mot attachment evaluation low-cycle fatigue estimates based on probabilistic approach. *ASME International Joint Power Generation Conference*, v. 2, pp- 51 1 - 5 16, 1996.
7. Millwater H. R. and Wu Y. T., Computational structural reliability analysis of a turbine bltz.de, *The American Society of Mechanical Engineers*. 93-GT-237, pp. 1- 14, 1993.
8. Srinivasan J., Gowda R- M. S. and Padmanabhan R., A numerical three dimensional thermal stresses analysis for cooled blades, *The American Society of Mechanical Engineers*, 89-GT- 168, pp. 1 - 4, 1989.
9. Arvantis S. T., Symko Y. B. and Tadros R. N., Multiaxial life prediction system for turbine components, *Journal of Engineering for Gas Turbines and Power*, Vol. 109, pp. 107 - 1 14, January 1987.
10. Hepworth J. K., Wilson J. D., Ailen J. M., Quentin G. H. and Touchton G., Life assessment of gus turbine blades and vanes, *The American Society of Mechanical Engineers*, 97-GT-446, pp. 1 - 6, 1997.
11. Amagasa S., Shimomura K., Kadowaki M., Takeishi K., Kawai H., Aoki S. and Aoyama K., Snuiy on the turbine vane and blade for a 1500" class industrial gas turbine, *The American Society of Mechanical Engineers*, 93-GT414, pp. 1 - 7, 1993.
12. Wan S. M., Lam T- C. T., Allen J. M. and McCloskey T. H., A gas turbine blade thennaUstructural program with linked flow-solid modeling capability, *The American Society of Mechanical Engineers*, 94-GT-270. OD. 1 - 7, 1994.
13. Masataka M., Yasutomo K., Thom K, Katsuhisa F., Yoshiki K. and Seigo L, Root and Groove Contact Analysis for Steam Turbine Blades. *Japan Society of Mechanical Engineers International Journal, Series I: Solid Mechanics and Strength of Materials*, v. 35, No. 4, pp. 508 - 514, 1992.
14. Zboinski G., Physical and geometrical non-linearity's in contact problems of elastic turbine blade attachments, *Proceedings of the Institute of Mechanical Engineers: Part C: Journal of Mechanical Engineering science*, v. 209, N. C4, pp. 273 - 286, 1995.
15. Mase M., Kaneko Y. and Watanabe E., Study on the contact technology and optimal figure design of the roof and groove for steam turbine long blades, *International Conference on Computer Aided Optimum Design of Structures, OPTI, Proceedings, Computational Mechanics Publications, Southampton, United Kingdom*, pp. 489 - 498, 1997.
16. Srivastav S. and Redding M., 3D Modelling of irnperject contact conditions between turbine blades and disk, *Advances in Steam Turbine Technology for the Power Generation Industry: ASME International Joint Power Genetarion Conference*, v. 26, pp. 197 - 204, 1994.
17. Uchino K., Kamiyarna T., Inarnura T., Simokohge K., Aono H. and Kawashima T., Three-dimensional photoelastic analysis of aeroengine rotary parts, *Proceeding of the International Symposium on Photoelasticity, Tokyo*, pp. 209-214, 1986.
18. Durelli A. J. and Rajaiah K., Lighter and stronger. *Experimental Mechanics*, pp. 369 - 379, November 1980.
19. Parks V. I. and Sandford R. I., Photo elastic und holography analysis of a turbine-engine component, *Experimental Mechanics*, pp. 328 - 333, September 1978.
20. Haake S. J., Patterson E. A. and Wang 2. F., 20 and 30 separation stresses using automated photo elasticity, *Experimental Mechanics*, Vol. 36, no. 3, pp. 269 - 276, September 1996.